Available online at www.sciencedirect.com
ScienceDirect
Trans. Nonferrous Met. Soc. China 31(2021) 1599−1611
Transactions of Nonferrous Metals Society of China
www.tnmsc.cn

Effect of ECAP process on liquid distribution of AZ80M alloy during semi-solid isothermal heat treatment

Ling-ling FAN[1], Ming-yang ZHOU[2], Yang-yang GUO[1], Yu-wen-xi ZHANG[1], Gao-feng QUAN[1]

1. Key Laboratory of Advanced Technologies of Materials, Ministry of Education, School of Materials Science and Engineering, Southwest Jiaotong University, Chengdu 610031, China;
2. Science and Technology on Reactor System Design Technology Laboratory, Nuclear Power Institute of China, Chengdu 610213, China

Received 27 June 2020; accepted 6 April 2021

Abstract: Two kinds of semi-solid samples of AZ80−0.2Y−0.15Ca (wt.%) (AZ80M) magnesium alloy were prepared by semi-solid isothermal heat treatment of materials with and without equal channel angular pressing (ECAP) process. The microstructures of initial and semi-solid treated samples were compared and analyzed. The results showed a significant difference in the liquid phase distribution between three-pass ECAP processed (3P) and as-received samples during the isothermal heating process. The semi-solid 3P sample showed a more uniform liquid distribution due to its smaller dihedral angle. Besides, the coarsening processes of solid grains of as-received and 3P samples were dominated by the coalescence and Ostwald ripening mechanism, respectively. The difference of coarsening processes was mainly related to the proportion of the high-angle grain boundaries in materials, which further affected the evolution behavior of the liquid pools.

Key words: AZ80M; equal channel angular pressing; semi-solid microstructure; liquid phase distribution; coarsening mechanism

1 Introduction

Magnesium alloys have been considered as promising light metals in aerospace, rail transportation and automobile because of their low density, high specific strength and stiffness, machinability, and good recyclability [1]. Thixo-forming, a semi-solid processing (SSP) method, has many apparent advantages compared with conventional casting and forging, including the ability to produce a more compact structure with fewer solidification defects, as well as a near-net-shape forming capability and a prolonged die life [2−4]. The critical issue of thixoforming is preparing a semi-solid billet with a fine and spheroidal microstructure, which can be obtained by recrystallization and partial melting (RAP) or strain-induced melt activation (SIMA) method to apply plastic deformation to the initial billet [5]. Using severe plastic deformation (SPD), such as equal channel angular pressing (ECAP), in the SIMA route to obtain highly-strained material before partial remelting, is the most effective way to acquire fine and spheroidal grains accompanied by more liquid [6].

Many studies have shown that solid grains with a smaller size and a higher roundness, and a sufficient liquid phase uniformly distributing among them are beneficial to improving thixoforming performance [7−9]. Up to now, although much work has been devoted to study the effects of preparation processing parameters of the billet on semi-solid microstructure, these studies

Corresponding author: Gao-feng QUAN, Tel: +86-13980066985, E-mail: quangf@swjtu.edu.cn
DOI: 10.1016/S1003-6326(21)65601-7

were mainly focused on the size, roundness and coarsening rate of the solid grains [10−15]. Nevertheless, there are rare documents on the liquid phase, which plays a significant role in the thixoforming process in fact. The liquid phases in semi-solid microstructure are divided into the intragranular and intergranular liquid phase, termed as “the liquid droplet or pool” and “the liquid film”, respectively. The existence of coarse liquid pools usually leads to the formation of micro-porosity and thus impairs the mechanical properties of thixotropic products [16,17], while the liquid phase outside the solid grains can provide a lubrication action during thixoforming process [18]. However, if the liquid phase gathers at the triangular grain boundaries, even outside the solid grains, it cannot play a lubricating role. Therefore, the sufficient and uniform liquid phase between solid grains is the key to ensuring the proceeding of the thixoforming process and the high quality of thixotropic products.

Many researchers suggested that the liquid distribution was determined by the dihedral angle (Φ) [19−22]. The Φ value is a crucial physical parameter representing an angle between two adjacent solid grains in contact with the liquid phase [20], as illustrated schematically in Fig. 1. The smaller the dihedral angle is, the more deeply the liquid phase penetrates into the grain boundary (GB), which is more conducive to the formation of a continuous liquid network structure [23,24]. Therefore, the average dihedral angle of the semi-solid system determines the permeability of liquid networks and liquid distribution under a certain volume fraction of the liquid phase. WALTE et al [22] suggested that an interconnected liquid network would form when the Φ value was lower than 60°, even if the liquid volume fraction was far smaller than 1 vol.%. However, when the Φ value was above 60°, the liquid phase would stay at triangular grain boundaries and fail to form a continuous liquid network. In addition, the liquid phase in the high Φ system tended to be non-uniformly distributed; in contrast, the liquid phase distribution in the low Φ system was much more uniform. Although these researchers concluded that the liquid distribution was related to the Φ value, no detailed studies have been conducted regarding the liquid distribution and the Φ value of SPD-treated magnesium alloys in a semi-solid system. Investigations on the effect of SPD on the liquid distribution of alloy during semi-solid isothermal heat treatment will provide valuable guidance for the application of the SSP technology.

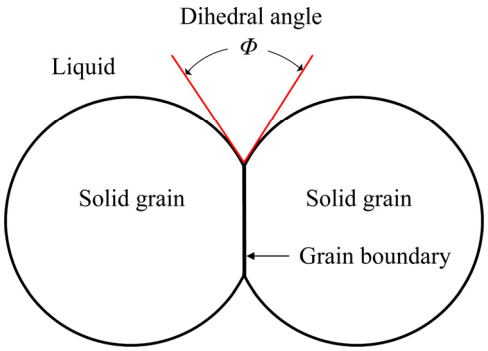

Fig. 1 Diagram of dihedral angle for solid−liquid system [20]

Accordingly, this work aims to provide insight into the effect of the ECAP process on the liquid distribution of AZ80−0.2wt.%Y−0.15wt.%Ca (AZ80M) during isothermal semi-solid treatment. Semi-solid billets of the AZ80M magnesium alloy were prepared using different passes of ECAP followed by a semi-solid isothermal heat treatment. Subsequently, the optimal semi-solid billets were selected according to the semi-solid microstructure characteristics. For comparison, the as-received materials were also subjected to the same semi-solid heat-treatment process. In order to clarify the influence of the ECAP process on the liquid phase distribution, the original and semi-solid microstructures of the alloy employing the ECAP process or not were analyzed comparatively. Finally, the evolution mechanisms of the liquid phase in the alloys undergoing two treatments were also discussed.

2 Experimental

2.1 Material and process

The starting materials used in this work were extruded rods (d30 mm) of AZ80−0.2Y−0.15Ca (wt.%) (AZ80M) magnesium alloy. The extrusion temperature and extrusion ratio were 350 °C and 9:1, respectively. The purpose of adding Y and Ca elements is to improve the quality of billets, which can refine grains and improve the high-temperature performance and flame-retardancy of magnesium

alloys [25,26]. Their chemical composition is listed in Table 1, which was tested using inductively coupled plasma-atomic emission spectrometry (ICP-AES) [27].

Table 1 Chemical composition of AZ80M magnesium alloy (wt.%)

Al	Zn	Y	Ca	Mg
6.76	0.33	0.19	0.073	Bal.

The cubic specimens with dimensions of 20 mm × 20 mm × 70 mm for ECAP deformation were cut from the center of extruded rod, as shown in Fig. 2(a). These cubic samples were subjected to one pass, two passes, three passes or four passes of ECAP using route Bc at (320±5) °C, which was termed as "1P", "2P", "3P" and "4P" samples, respectively. The ECAP die was made of H13 steel with an internal angle of 90° and external angular of 37°. A heating jacket was placed around the die and a thermometer was put inside the die to control the extrusion temperature. Before ECAP, the cubic specimens were preheated at 320 ℃ for 15 min in a resistance furnace. Both the die and specimens were lubricated by molybdenum disulfide (MoS_2) to reduce friction. After each pass of ECAP, the deformed specimens were immediately quenched in cold water.

The samples for the semi-solid isothermal treatment were cylinders with a diameter of 8 mm and a height of 12 mm, which were cut from the ECAP deformed specimens parallel to the extrusion direction, as shown in Fig. 2(b). The isothermally treated samples were heated to different semi-solid temperatures (560, 580 and 600 °C) in a PID-controlled resistance furnace, with the temperature of the samples monitored using a K-type thermometer. The selection of the semi-solid temperature range has been carefully described in our previous study based on DSC curve analysis [27]. Before heating, a sufficient amount of FeS was put in the resistance furnace to prevent the sample from oxidizing or even burning during the heating process. After the electric resistance furnace reached the target temperature for 10 min, the separate samples were put into the furnace and held for 10−30 min separately. Finally, the semi-solid heat-treated samples were immediately taken out for water quenching to keep the semi-solid microstructure.

2.2 Microstructure characterization

The microstructure observation surfaces of all samples were perpendicular to the extrusion direction in this study. The samples were polished and etched with the picric acid solution (2.75 g picric acid, 2.5 mL acetic acid, 45 mL ethyl alcohol, and 5 mL distilled water). The microstructure of as-received and ECAP processed samples after semi-solid isothermal heat treatment were observed using an optical microscope (OM, ZEISS Axio Lab. A1). The initial microstructure of as-received and

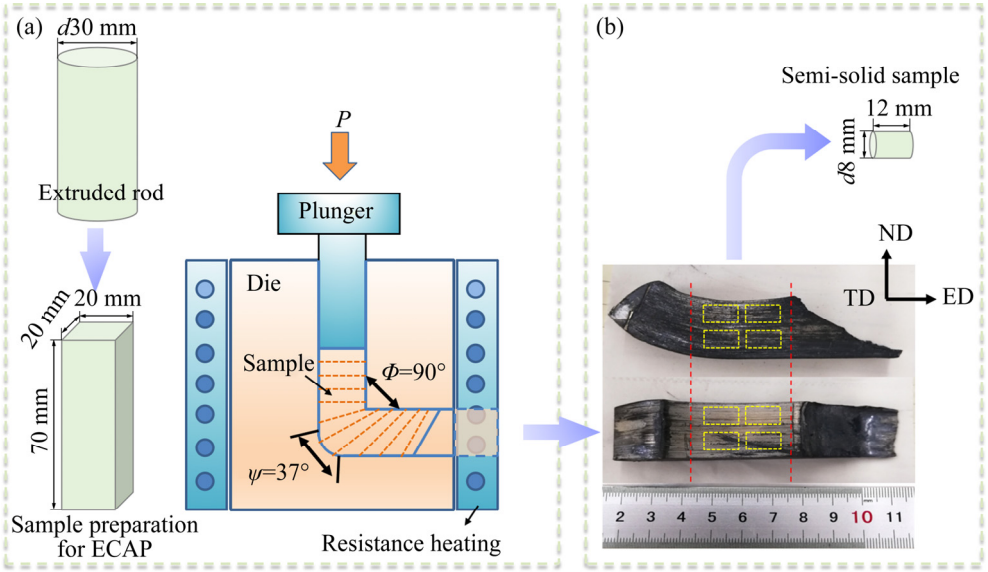

Fig. 2 Schematic diagrams of ECAP die and sample preparation for ECAP (a) and sampling of semi-solid specimen from ECAP processed sample (b)

ECAP processed samples were characterized using a field emission scanning electron microscope (FESEM, JEOL JSM 7800F) equipped with electron back-scattered diffraction (EBSD, Oxford Instrument Nordlys Nano) detector. The microstructural features, such as grain size distribution, misorientation angle distribution, and grain boundary character distribution, were analyzed using HKL channel 5 data acquisition software. The Image-Pro Plus software was utilized to measure and analyze the average size of solid grain (D), the liquid film thickness (δ) and the volume fraction of the effective liquid phase (the volume fraction of liquid film, f_L). The D and δ values were estimated using the mean linear intercept method based on the optical micrograph. At least three images were used for statistical analysis. The f_L value was calculated by the following equations:

$$f_L = 1 - \frac{1}{S}\sum_{i=1}^{n} A_n \quad (1)$$

where A_n is the area of the solid grain, S is the area of the optical graph, and n is the number of solid grains.

3 Results and discussion

3.1 Initial microstructure

Figure 3 shows IPF maps and corresponding grain size distribution of as-received and ECAP processed samples. After the first pass, the refinement of grain size was marginal, but an apparent reduction in the grain size distribution could be observed as the number of ECAP passes increased from one to three. Moreover, the grain size distribution profile became narrow and the grain size tended to be more uniform with an increase in the number of ECAP passes from one to three. However, further increasing the number of ECAP passes to four led to an increase in grain size.

3.2 Semi-solid microstructure

To select the optimal semi-solid billet, semi-solid microstructures of as-received and 1P−4P alloys subjected to isothermal heating at 580 °C for 10−30 min were compared, as presented in Fig. 4. After the semi-solid isothermal heating at 580 °C for 10−30 min, the size of solid grain of the 1P sample was larger than that of the as-received sample. As the number of ECAP passes increased to three, the size of solid grain decreased gradually. But, further increasing to four passes resulted in a slight increase. Therefore, when the ECAP processed samples were isothermally heated at 580 °C for 10−30 min, the size of solid grain of the 3P sample was the smallest. The volume fraction of liquid film showed the ascending trend with the increase in the number of ECAP passes. It can be seen from the liquid distribution in Fig. 4(c, f, i, l, o) that, the amount and uniformity of liquid phase among solid grains increased with increasing the number of ECAP passes from one to three. This was primarily due to the transition from the coalescence mechanism to Ostwald ripening mechanism, which was beneficial to forming of liquid phase among solid particles. When the number of ECAP passes increased continuously to four, the uniformity of liquid film distribution slightly decreased. It was mainly because the higher nonuniformity of the grain size in the 4P sample promoted the Ostwald ripening process, resulting in more liquid phase and inhomogeneous liquid distribution [28].

Although the liquid film fraction of the 4P sample subjected to semi-solid isothermal heating was the highest, some coarsen liquid pools (marked by yellow arrows) existed in solid grains, obvious local liquid aggregation occurred among the solid grains, and some solid grains coarsened significantly, as shown in Fig. 4(o). Based on previous researches [29−31], the semi-solid microstructure with these characteristics was disadvantageous to the mechanical properties of thixoforming products. Therefore, the semi-solid microstructure of the 3P sample was desirable because of the small size of solid grains, the high volume fraction of the effective liquid phase, and the uniformity of liquid phase distribution among the solid grains.

3.3 Liquid phase distribution and evolution

Figure 5 shows the semi-solid microstructures of the as-received and 3P samples after heating at 560 and 600 °C for 10−30 min. When the as-received sample was heated at 560 °C for 10 min, most of the solid grains still stuck together accompanied by a limited liquid phase (Fig. 5(a)). With the holding time prolonging from 20 to 30 min

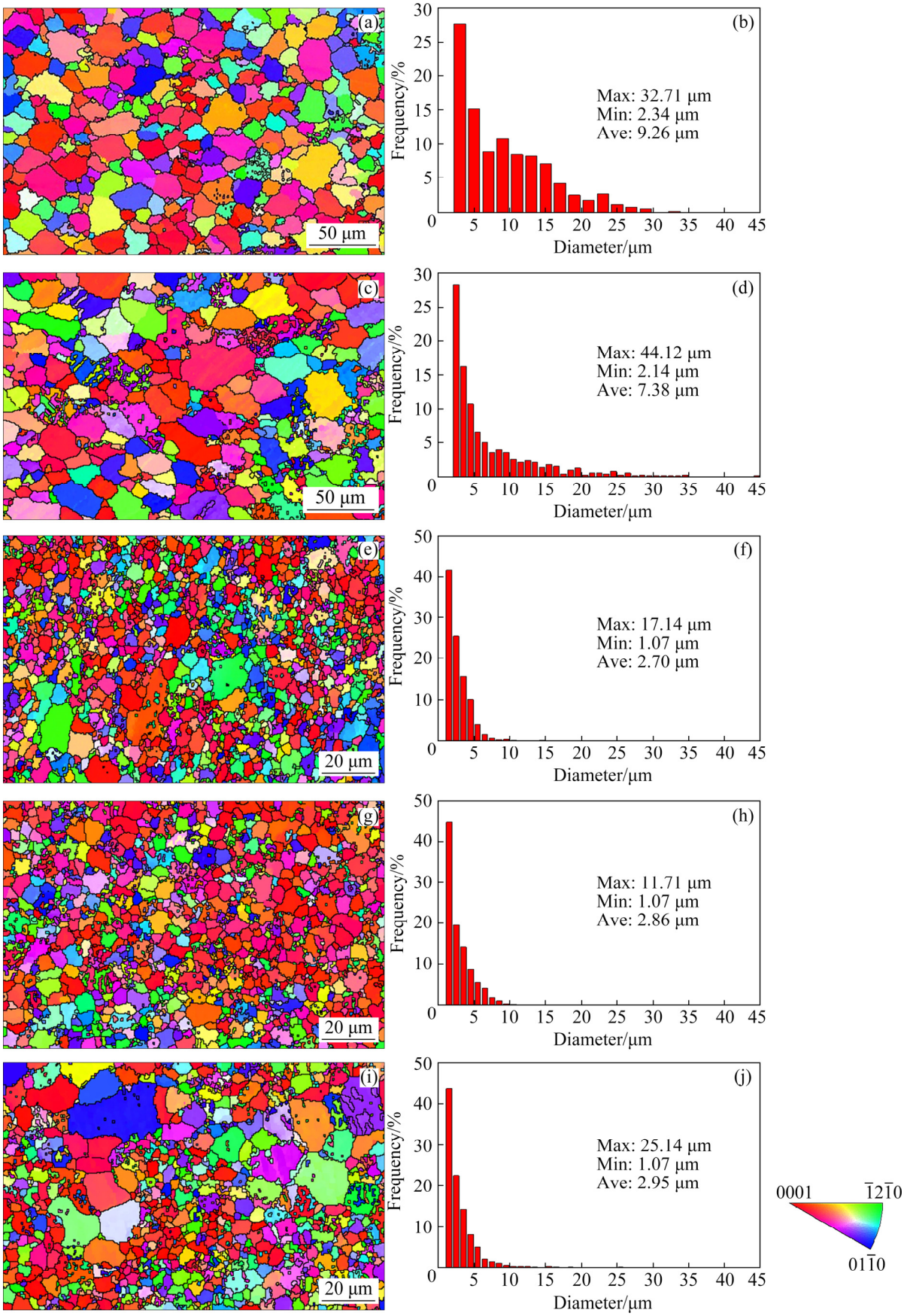

Fig. 3 EBSD inverse pole figure (IPF) maps (a, c, e, g, i) and corresponding grain size distribution (b, d, f, h, j) of as-received (a, b), 1P (c, d), 2P (e, f), 3P (g, h) and 4P (i, j) samples

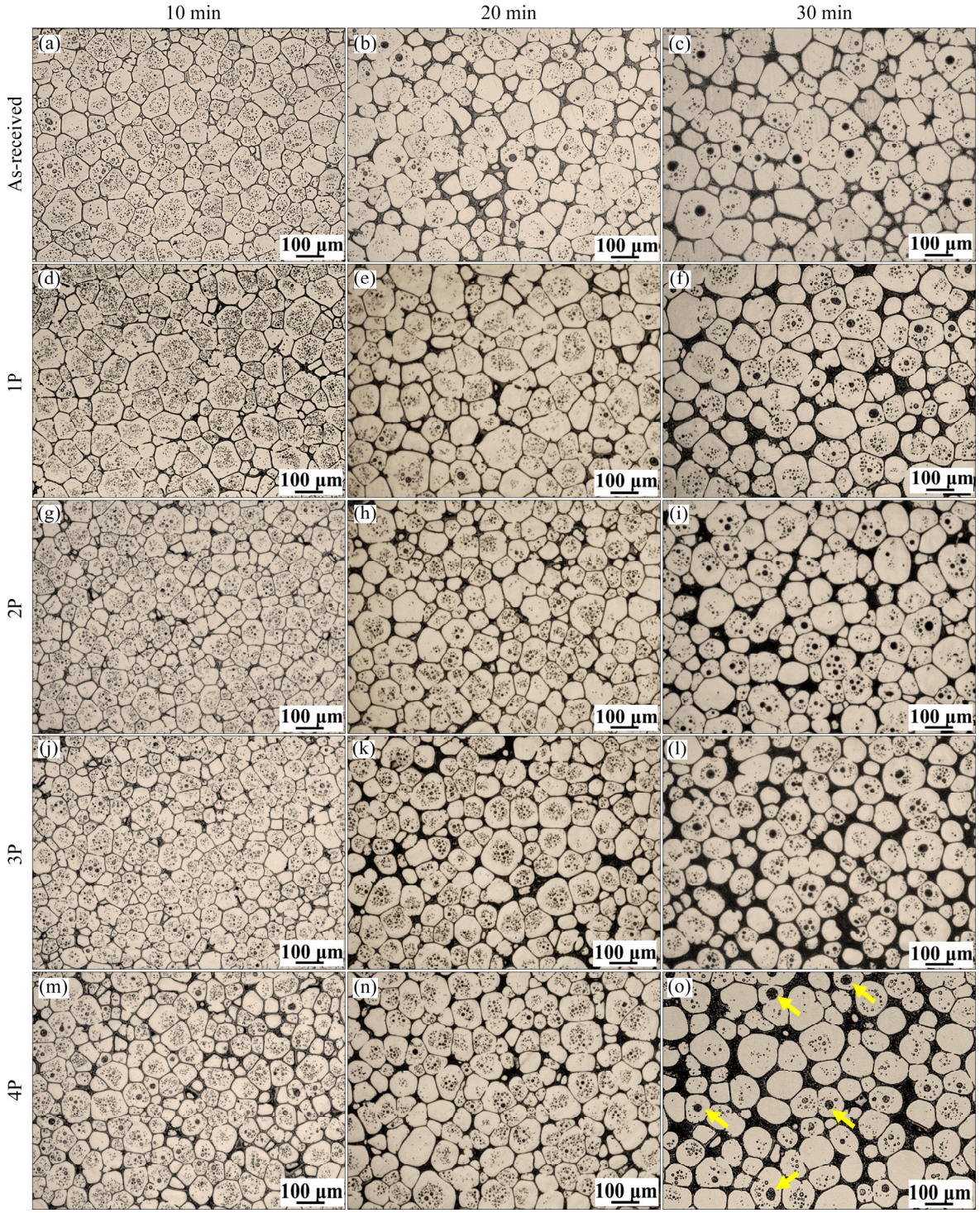

Fig. 4 Semi-solid microstructures of as-received and 1P−4P samples subjected to isothermal heating at 580 °C for 10, 20 and 30 min

(Figs. 5(b, c)), the combination phenomenon of solid grains was not significantly improved, and the liquid phase was mainly distributed at the triangular boundary. When the 3P sample was heated at 560 °C for 10 min (Fig. 5(d)), a continuous liquid film appeared around almost all solid grains. Moreover, the number of connected grains of the 3P sample was significantly lower than that of the as-received sample. With the increase of holding time from 20 to 30 min (Figs. 5(e, f)), the liquid film gradually widened in the 3P sample.

When the isothermal temperature was 600 °C and maintained for 10 min, the number of coarse liquid pools in the 3P sample was more than that in

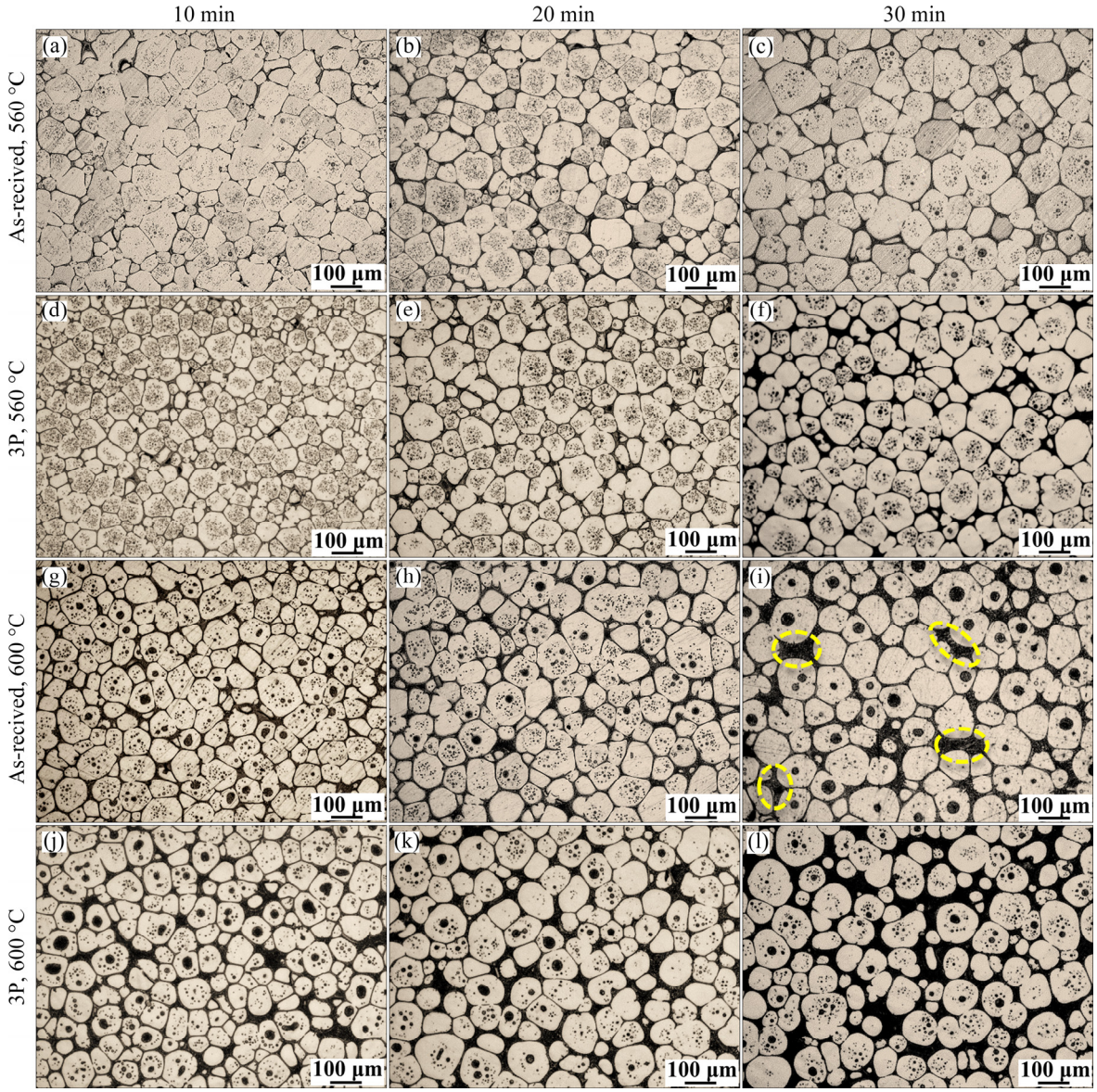

Fig. 5 Evolution of liquid phase distribution of as-received and 3P samples subjected to isothermal heating at 560 and 600 °C for 10, 20 and 30 min

the as-received sample, as represented in Figs. 5(g, j). For the as-received sample, as the holding time extended from 10 to 30 min (Figs. 5(g−i)), the liquid pools became coarser and the number of coarse liquid pools increased markedly. Although the volume fraction of liquid film increased, its distribution was inhomogeneous and even liquid separation existed (marked by yellow ellipses in Fig. 5(i)). However, for the 3P sample, extending the holding time from 10 to 30 min (Figs. 5(j−l)) resulted in the appreciable descending of the number of coarse liquid pools and the visible ascending of liquid film fraction. In general, after the same semi-solid heat treatment process, there were apparent differences in the distribution and evolution of liquid phase between as-received and 3P samples.

3.4 Relationship between liquid distribution and dihedral angle

According to previous research, the dihedral angle (Φ) was related to the distribution of the liquid phase [19−22]. The smaller Φ contributed to separating adjacent solid grains in the liquid phase, which then promoted the formation of the liquid film in the form of a continuous network structure surrounding the solid grains. Therefore, based on the results of previous studies and combined with

the phenomenon of Fig. 5 in this study, it can be speculated that the Φ value of the 3P sample was lower than that of the as-received sample in the same semi-solid heat-treatment process (at 560−600 °C for 10−30 min). In order to verify the speculation, the Φ value of as-received and 3P samples in the semi-solid system would be calculated subsequently.

As GERMAN [32] reported, the relationship among the contiguity (C_{SS}), the dihedral angle (Φ) and the volume fraction of solid phase (f_S) in the semi-solid alloy, can be expressed as

$$C_{SS}=f_S^2[0.43\sin\Phi+0.35\sin^2\Phi] \quad (2)$$

So, the Φ value can be calculated by obtaining C_{SS} and f_S.

The contiguity (C_{SS}) is a typical quantitative parameter for the microstructural characteristics of semi-solid materials. It reflects the degree of mutual contact among solid grains in the semi-solid system [32]. Generally, the C_{SS} value can be measured by quantitative micrograph using the intercept method, which can be expressed as [33]

$$C_{SS}=\frac{2N_{SS}}{2N_{SS}+N_{SL}} \quad (3)$$

where N_{SS} is the number of intersection points between the truncation line and solid−solid interface, and N_{SL} is the number of intersection points between the truncation line and solid−liquid interface.

ROEBUCK and ALMOND [34] considered the effects of solid volume fraction, the thickness of the liquid film and the size of solid grains based on measuring C_{SS} by the transversal method:

$$\frac{\delta}{D}(1-C_{SS})=\frac{f_L}{f_S} \quad (4)$$

where δ is the thickness of the liquid film, D is the average size of solid grains, f_S represents the volume fraction of the solid phase, and f_L represents the volume fraction of the effective liquid phase (the volume fraction of liquid film).

According to Eq. (4), the C_{SS} values were calculated, as shown in Fig. 6(a). With the increase of the holding time and isothermal temperature, the C_{SS} values of the as-received and 3P samples gradually decreased. Meanwhile, the C_{SS} value of the 3P sample was lower than that of the as-received sample, indicating a lower solid−solid contact degree of semi-solid microstructure in the 3P sample, which was in accordance with the micrograph in Fig. 5.

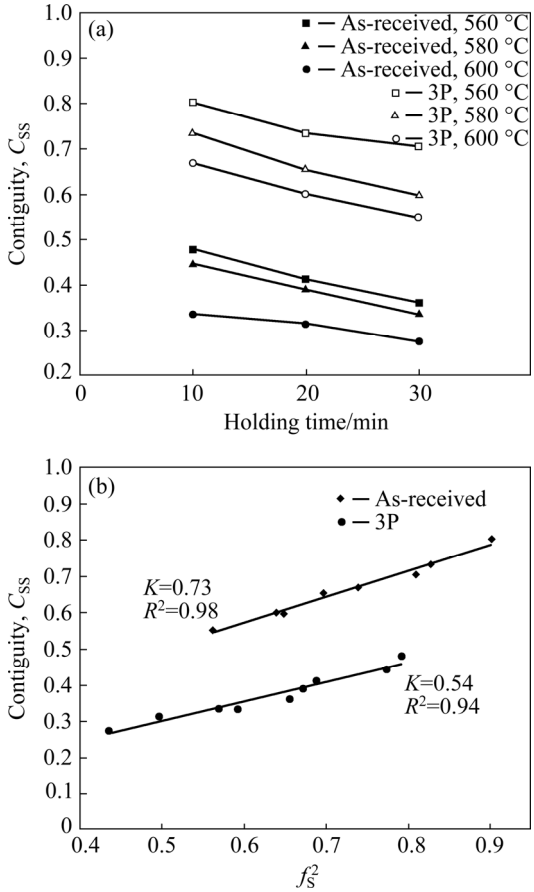

Fig. 6 Contiguity (a) and relationships of contiguity (C_{SS}) and square of solid volume fraction (f_S^2) (b) of as-received and 3P samples subjected to isothermal heating at 560−600 °C for 10−30 min

According to Eq. (2), the relationships of contiguity (C_{SS}) and the square of solid volume fraction (f_S^2) were linear fitted to calculate the Φ value. As plotted in Fig. 6(b), there was an excellent linear correlation between C_{SS} and f_S^2. For as-received and 3P samples, the linear slopes of C_{SS}− f_S^2 could be obtained as 0.73 and 0.54, and then the corresponding Φ value was calculated as 72.7° and 50.4°, respectively. The calculation results confirmed the previous speculation that the semi-solid microstructure of the 3P sample possessed a lower Φ value than the as-received sample. Therefore, the liquid phase in the 3P sample tended to be distributed homogeneously among the solid grains rather than segregating inside or outside the solid grains. This result was consistent with the previously published studies

performed by HAGHDADI et al [19] and WALTE et al [22]. For a semi-solid system with low Φ, the liquid would tend to spread over the surface of the grain boundary. However, for a semi-solid system with high Φ, the liquid would remain in the form of droplets at the trigeminal grain boundary or inside the solid-grains [19].

3.5 Mechanism of liquid phase evolution

The dihedral angle between two adjacent solid grains depends on the ratio of solid/solid and solid/liquid interfacial energy, and the relationship can be expressed by the following formula [20]:

$$2\cos(\Phi/2)=\gamma_{SS}/\gamma_{SL} \quad (5)$$

where γ_{SS} is the solid/solid grain boundary (GB) energy, and γ_{SL} is the solid/liquid interfacial energy. Whether the liquid phase penetrates into GB depends on the condition of $2\gamma_{SL}\leq\gamma_{SS}$ [19]. In general, grain boundary energy between adjacent solid grains is dependent on the misorientation angle (θ) between them. High-angle grain boundaries (HAGBs, $\theta\geq15°$) usually have larger GB energy than low-angle grain boundaries (LAGBs, $2°\leq\theta<15°$), so HAGBs are easier to satisfy the condition of being infiltrated by the liquid phase [30]. Therefore, in the initial stage of semi-solid isothermal heating, liquid films appear preferentially at these HAGBs. However, the adjacent solid grains with LAGBs cannot be separated by liquid and thus tend to grow by coalescence mechanism [30,35]. Therefore, the type of grain boundaries (GBs) in the initial microstructure plays a vital role in the formation and distribution of the liquid phase in the early stage of semi-solid isothermal heating.

Figure 7(a) shows the misorientation angle distribution of the as-received and 3P samples. It can be seen that the fraction of HAGBs of 3P sample (72.5%) was significantly higher than that of the as-received sample (53.0%). Figures 7(b, c) reveal the grain boundary distribution images of the as-received and 3P samples, respectively. The green lines and black lines correspond to LAGBs and HAGBs, respectively. Green lines (LAGBs) became much sparser in the microstructure of the 3P sample. In short, the 3P sample had a higher proportion of HAGBs. Figure 8 shows the liquid film distributions of as-received and 3P samples isothermally heated at 580 °C for 2 min. For the

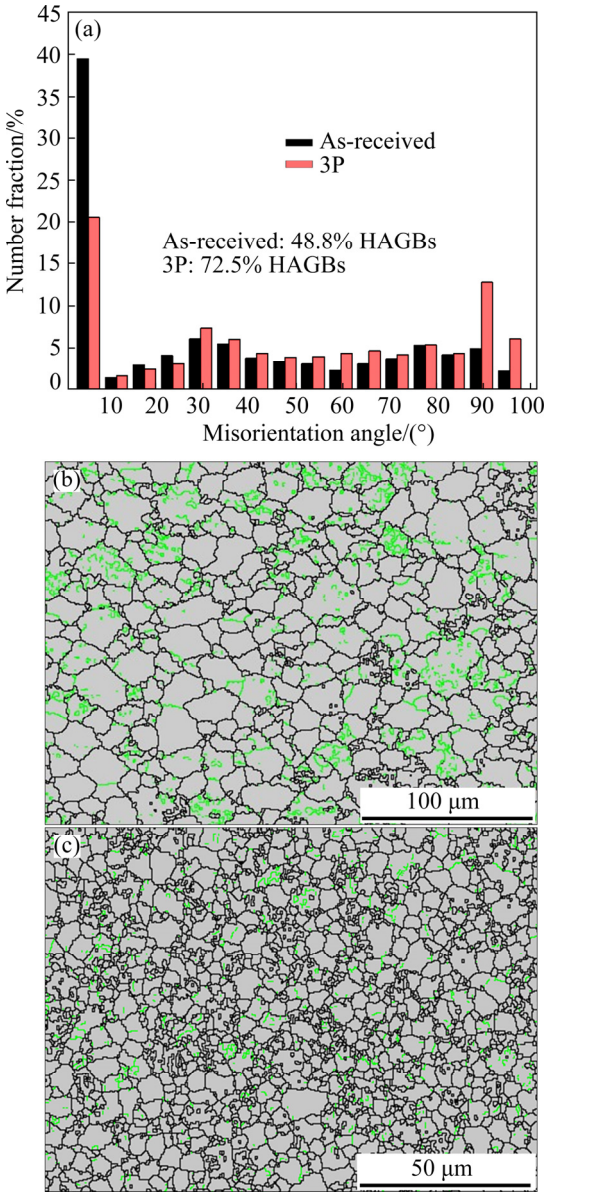

Fig. 7 Misorientation angle distribution (a) and grain boundary distribution images of as-received (b) and 3P (c) samples

as-received sample, only a few grain boundaries were infiltrated by the liquid phase, and the liquid film was discontinuous without forming a network structure. However, for 3P sample, the continuous liquid film preferentially formed. Therefore, it can be concluded that the large proportion of HAGBs was conducive to the formation of the continuous liquid film around the solid grains in the initial stage of semi-solid isothermal heating.

With the further increase of the holding time or isothermal temperature for as-received samples, a substantial number of the adjacent solid grains could not be infiltrated by the liquid phase as the

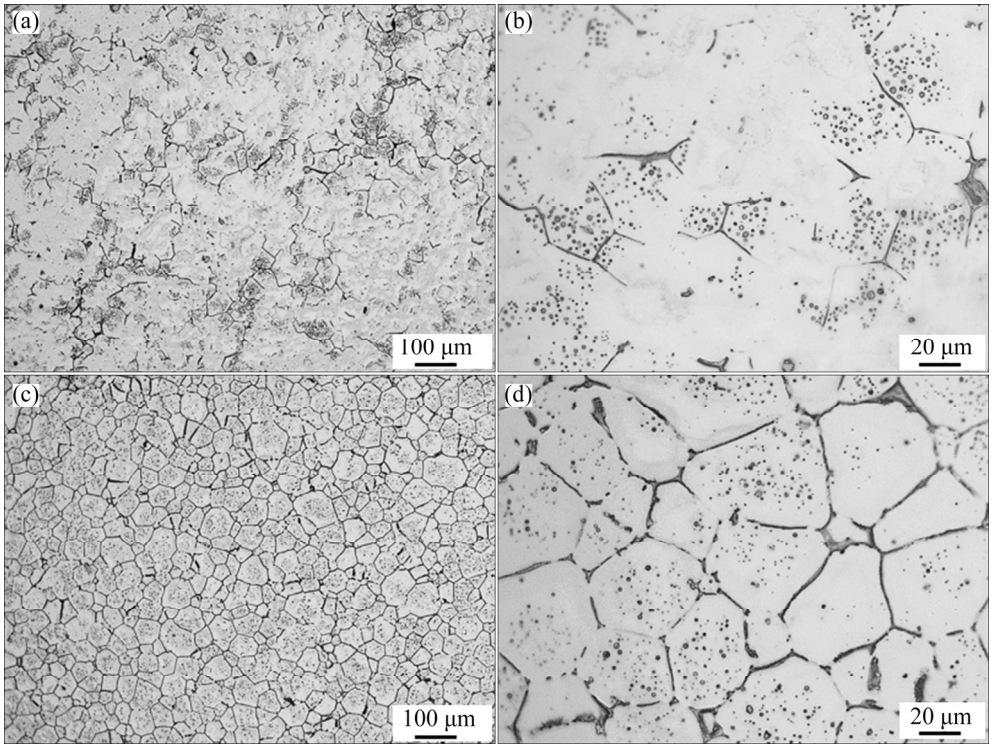

Fig. 8 Liquid film distributions of as-received (a, b) and 3P (c, d) samples subjected to isothermal heating at 580 °C for 2 min

result of a small proportion of HAGBs. Moreover, adjacent solid grains were extremely prone to merge and form an irregular and coarse grain due to their low misorientation angle. In this case, the coalescence mechanism dominated in the coarsening process of solid grains in the as-received sample during semi-solid isothermal heat treatment. Coalescence is a coarsening process in which two adjacent solid grains combine to form one solid grain with a complex geometric shape during the semi-solid heat treatment, resulting in reduced solid−liquid interface energy [36]. Therefore, the liquid pools were more likely to remain in the center of the merged grain. This could explain why the increase of holding time led to an increase in the number of coarse liquid pools inside the solid grains when the as-received samples were heated at 600 °C (Figs. 5(g−i)). Besides, previous researches have shown that some liquid phase may be carried into the coarse and irregular grains in the process of coalescence, increasing the intragranular liquid pools [7,37].

When a 3P sample with a large proportion of HAGBs was heated isothermally at a semi-solid temperature, firstly, most of the GBs were penetrated by the liquid phase. Then, a substantial amount of solid grains were completely isolated and wrapped by a continuous liquid film. In this case, the Ostwald ripening mechanism dominated in the coarsening process of solid grains in the 3P sample during semi-solid isothermal heat treatment. The Ostwald ripening is a coarsening process in which large grains grow by consuming small grains when the sizes of two globular grains differ greatly. It is controlled by the Gibbs−Thompson effect, which changes the concentration of the solid−liquid interface according to the curvature of the interface, thereby creating a concentration gradient and leading to the diffusion of the material [38]. The solute around the boundary of the large solid grain transfers to the surrounding of the boundary of the small grain [38]. Thus, in the process of Ostwald ripening, small solid grains gradually melt due to the increase in solute concentration around the boundary of them, which promotes the formation of liquid channels around the solid grains. It also can be confirmed by Fig. 5(l), many small solid grains exited in the liquid-rich region. However, for large solid grains, they would continue to spheroidize and grow owing to the decrease in solute concentration around their boundary, resulting in the increase of solid−liquid interface energy of large solid grains.

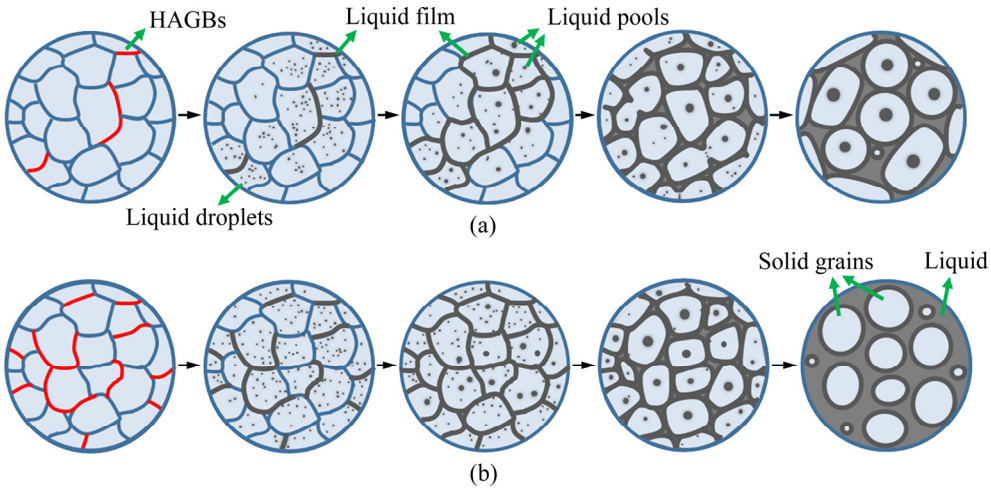

Fig. 9 Schematic illustration showing semi-solid microstructure evolution for as-received (a) and 3P (b) samples

In order to reduce the solid−liquid interface energy of large solid grains, the liquid droplets or liquid pools near the liquid film would first migrate to the liquid film, while those far away from the liquid film would merge, spheroidize, and finally migrate to the liquid film through the solute transport under the driving of the increase of solid−liquid interface energy. Similar findings were also reported by other researchers [7,19,39]. Consequently, the number of the liquid pools reduced and the thickness of the liquid film further increased, which could be confirmed by micrographs of the semi-solid microstructure evolution of the 3P samples in Figs. 5(j−l).

Based on the above discussion and analysis, a schematic diagram of the liquid phase evolution of the as-received and 3P alloy during semi-solid isothermal heat treatment is given in Fig. 9. It can be concluded that the proportion of HAGBs had a significant influence on the dominant coarsening mechanism in subsequent semi-solid heating. Then, different coarsening mechanisms would lead to different changes in the solid−liquid interface energy of solid grains, thereby affecting the evolution of the liquid pools inside solid grains. Therefore, the formation of effective liquid phase depended on the type of GB and the coarsening mechanism. To obtain a semi-solid billet with sufficient and effective liquid fraction, it is necessary to gain the initial microstructure with a high proportion of HAGBs and a large number of fine grains with uniform distribution simultaneously. The former facilitated most solid grains to be encapsulated in the liquid phase, which determined that the Ostwald ripening mechanism dominated in the subsequent coarsening process. Moreover, the latter was beneficial to the homogeneous distribution of the liquid phase and the increase of liquid fraction among solid grains.

4 Conclusions

(1) ECAPed (3P) sample had a smaller Φ value (50.4°) than the as-received sample (72.7°), resulting in more homogeneous and uniform liquid distribution among the solid grains.

(2) For the as-received sample, the coalescence mechanism dominated in the coarsening process, leading to the liquid pools tending to remain in the center of the combined solid grains.

(3) For the 3P sample, the Ostwald ripening mechanism dominated in the coarsening process, resulting in the migration of the liquid pools in large solid grains to the liquid film. Additionally, small solid grains continuously melted. These promoted an increase in the effective liquid fraction.

Acknowledgments

This work was supported by Key Development Project of Sichuan Province (Grant No. 2017GZ0399). Acknowledgements are given to the equipment support from Litmat Technology Chengdu Co., Ltd., China.

References

[1] REN Ling-bao, FAN Ling-ling, ZHOU Ming-yang, GUO Yang-yang, ZHANG Yu-wen-xi, BOEHLERT C J, QUAN Gao-feng. Magnesium application in railway rolling stocks:

A new challenge and opportunity for lightweighting [J]. International Journal of Lightweight Materials and Manufacture, 2018, 1: 81−88.

[2] XIAO Guan-fei, JIANG Ju-fu, WANG Ying, LIU Ying-ze, ZHANG Ying. Microstructure and mechanical properties of nickel-based superalloy GH4037 parts formed by thixoforming [J]. Materials Science and Engineering A, 2020, 780: 139196−139206.

[3] ARIF M A M, OMAR M Z, SAJURI Z, SALLEH M S. Effects of Cu and Mg on thixoformability and mechanical properties of aluminium alloy 2014 [J]. Transactions of Nonferrous Metals Society of China, 2020, 30: 275−287.

[4] LIU Jian, CHENG Yuan-sheng, CHAN S W N, SUNG D. Microstructure and mechanical properties of 7075 aluminum alloy during complex thixoextrusion [J]. Transactions of Nonferrous Metals Society of China, 2020, 30: 3173−3182.

[5] JIANG Ju-fu, WANG Ying, XIAO Guan-fei, NIE Xi. Comparison of microstructural evolution of 7075 aluminum alloy fabricated by SIMA and RAP [J]. Journal of Materials Processing Technology, 2016, 238: 361−372.

[6] FU Jin-long, JIANG Hong-jun, WANG Kai-kun. Influence of processing parameters on microstructural evolution and tensile properties for 7075 Al alloy prepared by an ECAP based SIMA process [J]. Acta Metallurgica Sinica (English Letters), 2018, 31: 337−350.

[7] CHEN-Qiang, ZHAO Zu-de, CHEN-Gang, WANG Bo. Effect of accumulative plastic deformation on generation of spheroidal structure, thixoformability and mechanical properties of large-size AM60 magnesium alloy [J]. Journal of Alloys and Compounds, 2015, 632: 190−200.

[8] ZHAO Zu-de, CHEN Qiang, TANG Ze-jun, HU Chuan-kai. Microstructural evolution and tensile mechanical properties of AM60B magnesium alloy prepared by the SIMA route [J]. Journal of Alloys and Compounds, 2010, 497: 402−411.

[9] JIANG Ju-fu, ATKINSON H V, WANG Ying. Microstructure and mechanical properties of 7005 aluminum alloy components formed by thixoforming [J]. Journal of Materials Science and Technology, 2017, 33: 379−388.

[10] CHU Chen-liang, HU Zhi, LI Xiao, YAN Hong, WU Xiao-quan, MAI Yuan-lu. Evolution and distribution of Al_2Sm phase in as-extruded AZ61−xSm magnesium alloys during semi-solid isothermal heat-treatment [J]. Transactions of Nonferrous Metals Society of China, 2018, 28: 1311−1320.

[11] MESHKABADI R, FARAJI G, JAVDANI A, POUYAFAR V. Combined effects of ECAP and subsequent heating parameters on semi-solid microstructure of 7075 aluminum alloy [J]. Transactions of Nonferrous Metals Society of China, 2016, 26: 3091−3101.

[12] BINESH B, AGHAIE-KHAFRI M. RUE-based semi-solid processing: Microstructure evolution and effective parameters [J]. Materials and Design, 2016, 95: 268−286.

[13] FU Jin-long, WANG Shu-xian, WANG Kai-kun. Influencing factors of the coarsening behaviors for 7075 aluminum alloy in the semi-solid state [J]. Journal of Materials Science, 2018, 53: 9790−9805.

[14] XU Yan, HU Lian-xi, JIA Jian-bo, XU Bo. Microstructure evolution of a SIMA processed AZ91D magnesium alloy based on repetitive upsetting-extrusion (RUE) process [J]. Materials Characterization, 2016, 118: 309−323.

[15] PRONI C T W, TORRES L V, HAGHAYEGHI R, ZOQUI E J. ECAP: An alternative route for producing AlSiCu for use in SSM processing [J]. Materials Characterization, 2016, 118: 252−262.

[16] TZIMAS E, ZAVALIANGOS A. Evolution of near-equiaxed microstructure in the semisolid state [J]. Materials Science and Engineering A, 2000, 289: 228−240.

[17] CAMPO K N, ZOQUI E J. Thixoforming of an ECAPed aluminum A356 alloy: Microstructure evolution, rheological behavior, and mechanical properties [J]. Metallurgical and Materials Transactions A, 2016, 47: 1792−1802.

[18] TANG Q, ZHOU Ming-yang, FAN Ling-ling, ZHANG Yu-wen-xi, QUAN Gao-feng, LIU Bing. Constitutive behavior of AZ80 M magnesium alloy compressed at elevated temperature and containing a small fraction of liquid [J]. Vacuum, 2018, 155: 476−489.

[19] HAGHDADI N, ZAREI-HANZAKI A, HESHMATI-MANESH S, ABEDI H R, HASSAS-IRANI S B. The semisolid microstructural evolution of a severely deformed A356 aluminum alloy [J]. Materials and Design, 2013, 49: 878−887.

[20] GERMAN R M, SURI P, PARK S J. Review: Liquid phase sintering [J]. Journal of Materials Science, 2009, 44: 1−39.

[21] DELANNAY F. The role of dihedral angle on the control of skeleton coordination and pore closure in aggregates driven by capillary forces [J]. Scripta Materialia, 2010, 62: 928−933.

[22] WALTE N P, BECKER J K, BONS P D, RUBIE D C, FROST D J. Liquid-distribution and attainment of textural equilibrium in a partially-molten crystalline system with a high-dihedral-angle liquid phase [J]. Earth and Planetary Science Letters, 2007, 262: 517−532.

[23] LIU Po-liang. The relation between the distribution of dihedral angles and the wetting angle during liquid phase sintering [J]. Computational Materials Science, 2006, 36: 468−473.

[24] LIU Jian-xin, GERMAN R M. Microstructure effect on dihedral angle in liquid-phase sintering [J]. Metallurgical and Materials Transactions A, 2001, 32: 165−169.

[25] REN Ling-bao, ZHOU Ming-yang, BOEHLERT C J, QUAN Gao-feng. Multi-microalloying mediated grain growth and texture evolution during the high-temperature static recrystallization of AZ80 alloys [J]. Journal of Alloys and Compounds, 2020, 834: 155077−155088.

[26] NAMIS B, MIRESMAEILI S M, JAMSHIDI F, KHOUBROU I. Effect of Ca addition on microstructure and impression creep behavior of cast AZ61 magnesium alloy [J]. Transactions of Nonferrous Metals Society of China, 2019, 29: 2056−2065.

[27] FAN Ling-ling, ZHOU Ming-yang, ZHANG Yu-wen-xi, TANG Qi, QUAN Gao-feng, LIU Bing. The semi-solid microstructural evolution and coarsening kinetics of AZ80−0.2Y−0.15Ca magnesium alloy [J]. Materials Characterization, 2019, 154: 116−126.

[28] FAN Ling-ling, ZHOU Ming-yang, REN Ling-bao, LI Hou-yi, ZHANG Hong-tao, LU Tian-hui, LIU Chong-liang, QUAN Gao-feng. The effect of equal channel angular pressing on coarsening kinetics of AZ80−0.2Y−0.15Ca alloy

in semisolid state [J]. Advanced Engineering Materials, 2020, 2000415−2000425.
[29] CHAYONG S, ATKINSON H V, KAPRANOS P. Thixoforming 7075 aluminium alloys [J]. Materials Science and Engineering A, 2005, 390: 3−12.
[30] JIANG Ju-fu, WANG Ying, ATKINSON H V. Microstructural coarsening of 7005 aluminum alloy semisolid billets with high solid fraction [J]. Materials Characterization, 2014, 90: 52−61.
[31] CHEN Gang, ZHOU Tao, WANG Bo, LIU Hong-wei, HAN Fei. Microstructure evolution and segregation behavior of thixoformed Al−Cu−Mg−Mn alloy [J]. Transactions of Nonferrous Metals Society of China, 2016, 26: 39−50.
[32] GERMAN R M. The contiguity of liquid phase sintered microstructures [J]. Metallurgical and Materials Transactions A, 1985, 16: 1247−1252.
[33] AMIRJAN M, PARVIN N, ZANGENEH-MADAR K. Mutual dependency of mechanical properties and contiguity in W−Cu composites [J]. Materials Science and Engineering A, 2010, 527: 6922−6929.
[34] ROEBUCK B, ALMOND E A. Deformation and fracture processes and the physical metallurgy of WC−Co hardmetals [J]. International Materials Reviews, 1988, 33: 90−112.
[35] RABKIN E, SNAPIRO I. Wetting of the low-angle grain boundaries [J]. Acta Materialia, 2000, 48: 4463−4469.
[36] ZHAO Zu-de, CHEN Qiang, WANG Yan-bing, SHU Da-yu. Microstructural evolution of an ECAE-formed ZK60−RE magnesium alloy in the semi-solid state [J]. Materials Science and Engineering A, 2009, 506: 8−15.
[37] LUO Shou-jing, CHEN Qiang, ZHAO Zu-de. Effects of processing parameters on the microstructure of ECAE-formed AZ91D magnesium alloy in the semi-solid state [J]. Journal of Alloys and Compounds, 2009, 477: 602−607.
[38] WANG Jin-guo, LIN Hua-qiang, WANG Hong-qing, JIANG Qi-chuan. Effects of different processing parameters on the semisolid microstructure of the AZ91D alloy during partial remelting [J]. Journal of Alloys and Compounds, 2008, 466: 98−105.
[39] CHEN Qiang, CHEN Gang, HAN Liu-na, HU Nan, HAN Fei, ZHAO Zu-de, XIA Xiang-sheng, WAN Yuan-yuan. Microstructure evolution of SiC_p/ZM6 (Mg−Nd−Zn) magnesium matrix composite in the semi-solid state [J]. Journal of Alloys and Compounds, 2016, 656: 67−76.

等径角挤压对 AZ80M 合金在半固态等温加热过程中液相分布的影响

范玲玲[1]，周明扬[2]，郭阳阳[1]，张钰雯茜[1]，权高峰[1]

1. 西南交通大学 材料科学与工程学院 材料先进技术教育部重点实验室，成都 610031；
2. 中国核动力研究设计院 核反应堆系统设计技术重点实验室，成都 610213

摘 要：将经过等径角挤压(ECAP)和未经 ECAP 的 AZ80−0.2Y−0.15Ca(质量分数，%)(AZ80M)合金试样进行半固态等温加热处理，得到两种半固态坯料。对两种坯料的在半固态等温加热处理前后的显微组织进行比较和分析。研究结果表明，在半固态等温加热处理中，经过 3 道次 ECAP(3P)后的试样与初始挤压态试样的液相分布明显不同。半固态处理后的 3P 试样具有更均匀的液相分布，这是因为其半固态系统中具有更小的二面角。另外，初始挤压态试样和 3P 试样的固相晶粒粗化过程分别由合并机制和奥斯瓦尔德熟化机制主导。这两种材料在半固态过程中显示出的不同粗化机制主要与大角晶界的占比有关，随着半固态过程的进行，不同的粗化机制会进一步影响液池的演变行为。

关键词：AZ80M；等径角挤压；半固态显微组织；液相分布；粗化机制

(Edited by Bing YANG)